A Comparative Study on the Performance of Marine Diesel Engines Running on Diesel/Methanol and Diesel/Natural Gas Mode

Weihe Yao[a], Yu Ding[a], Shuai Guan[a], Hongkai Ben[a], La Xiang[a*]

[a] Harbin Engineering University, Harbin, China
* Corresponding Author e-mail: xiangla@hrbeu.edu.cn

Abstract

With the increasingly stringent requirements of international decarbonization regulations, the shipping industry has accelerated the pace of exploiting low-carbon fuels. Methanol is one of the most prospective substitute fuels featured with low-carbon content, clean combustion and easy storage. For marine diesel/methanol dual-fuel engine applications, a certain quantity of diesel is typically used to ensure a stable ignition and combustion. However, the combustion and emission characteristics as well as the stable operation window of marine diesel/methanol dual-fuel engines under different operating loads have not yet been well investigated. In this study, a marine diesel/natural gas dual-fuel engine was used as a prototype to develop a 3D simulation model using CONVERGE, which was then validated using experimental data under different operating loads. The validated model was then employed to investigate the effects of methanol substitution rate (MSR) on the combustion and emission characteristics under the diesel/methanol operation mode. By monitoring the abnormal combustion phenomena such as misfire and knocking, the maximum MSR under different operating conditions was identified. Finally, the engine performances of diesel/natural gas and diesel/methanol modes were compared in terms of combustion and emission characteristics. The results show that the maximum MSR tends to increase first (from 5% to 43% under operation load from 25% to 75%) and then decrease (from 43% to 20% under operation load from 75% to 100%) with increasing operating load owing to the misfire limitation at low load and knocking limitation at high load, respectively. Comparing to the prototype diesel/natural gas mode, the diesel/methanol mode exhibited a shorter combustion duration with increased NOx emissions. The results obtained from this study are expected to guide the operation management of marine diesel/methanol dual fuel engines, and thus help reduce ships' CO_2 emissions.

Keywords: Diesel/methanol, Diesel/natural gas, Operating load, Combustion characteristics, Emissions, Substitution rate.

1. INTRODUCTION

With increasingly stringent emission regulations, a number of methods, such as using alternative fuels, optimizing the combustion process, and adding after-treatment equipment, have been employed to reduce carbon emissions in the marine shipping industry. Methanol is one of the most prospective alternative fuels for marine engines due to its low-carbon, clean-combustion, easy-storage and renewable characteristics [1].

When applied in internal combustion engines, methanol can be used alone [2-3] or in combination with other fuels, such as methanol-diesel engines, methanol-gasoline engines, methanol-hydrogen engines, etc [4-5]. For marine application, methanol-diesel engines are more widely used, which can be divided into three classifications: direct blending, port injection, and direct injection. Direct blending means methanol is emulsified and mixed with diesel to form a diesel-methanol mixture as an engine fuel [6-8]. Port injection methanol-diesel engine is to inject methanol into the intake port, where it is mixed with air before entering the cylinder during the intake process, while the diesel fuel is injected directly into the cylinder before the top dead center (TDC) for igniting the methanol [9-12]. Direct injection methanol-diesel engine is to inject both methanol and diesel directly into a cylinder. Two separate nozzles are used to inject methanol and diesel, with diesel generally injected before the TDC, while there are a number of methanol injection strategies [13-15]. However, the combustion and emission characteristics as well as the operational stability of marine diesel/methanol dual-fuel engines under different operating loads are seriously affected by misfire and knocking [16].

In this area, Duan et al. [3] investigated the causes of knocking in methanol engines, showing that the premature ignition due to hot spots causes severe knocking which can be suppressed by using a fractional direct in-cylinder injection strategy.

DOI: https://doi.org/10.59490/moses.2023.656

Yin et al. [13] investigated the effects of methanol direct injection strategies on engine performance. The results show that injection of methanol during the compression stroke could result in a large in-cylinder fuel concentration gradient, thus reducing the combustion duration. The ignition delay and combustion duration increased with the increase of methanol blending ratio, whilst the combustion stability was improved. Li et al. [16] compared the diesel/methanol dual-fuel engine knocking in port injection and direct injection mode. The results show that direct injection mode can effectively inhibit the occurrence of knocking, while the port injection mode is relatively serious, however, it can be suppressed by optimizing the diesel injection strategy or increasing exhaust gas recirculation. Sun et al. [17] improved the knocking of a diesel-methanol dual-fuel engine in direct injection mode based on the optimization of the in-cylinder injection strategy. The results show that the optimized injection strategy can improve the economy while reducing the intensity of knocking. To summarize, the research related to knocking has been relatively intensive, while the research related to misfire is still unclear.

Previous studies on methanol have been relatively comprehensive. However, in terms of evaluating misfire phenomenon, the most widely used index is the cyclic fluctuation rate of the indicated mean effective pressure (IMEP), which is inappropriate for CFD modelling within one cycle. Thus, a new method of misfire evaluation (PCC) is proposed in this study, which can provide new ideas for the operating boundary exploration of dual-fuel engines. In addition, methanol and natural gas are good choices for marine dual-fuel engines. The application technologies of the diesel/natural gas mode have been well developed, whilst those of the diesel/methanol mode are still under development. Therefore, it is of great significance to investigate the convention from diesel/natural gas mode to diesel/methanol mode.

To explore the combustion and emission characteristics as well as the steady operation window of a port injection marine diesel/methanol engine, a CFD model was chosen because of its high accuracy in predicting the knocking and misfire phenomena as well as engine emissions. By monitoring the abnormal combustion phenomena such as misfire and knocking, the maximum methanol substitution rate under different operating conditions was identified. Finally, the engine performances of diesel/natural gas and diesel/methanol modes were compared in terms of combustion and emission characteristics. This study can provide guidance for the conversion of diesel/natural gas dual-fuel engines to diesel/methanol dual-fuel engines and help reduce CO_2 emissions of ships in the future.

2. MODELLING METHODOLOGY

In this study, a 3D CFD simulation model was developed using CONVERGE software, which has the advantages of autonomous meshing and abundant sub-models. Since n-heptane can describe the ignition and combustion characteristics of diesel fuel well [31], it was chosen to simulate the diesel injection and combustion processes in this study. The properties of n-heptane and methanol are presented in Table 1.

Table 1. Properties of methanol and n-heptane

	Methanol	N-heptane
Molecular Formula	CH_3OH	C_7H_{16}
Molecular weight (g/mol)	32	100
Density（g/cm^3,at 20℃）	0.79	0.683
Boiling temperature (℃)	64.7	98.8
Flashpoint (℃)	11	-4
Auto-ignition temperature (℃)	470	204
Viscosity (mPa s at 298.15K)	0.59	0.4
Stoichiometric fuel-air ratio	0.154	0.069
Cetane number	3-5	56
Lower heating value (MJ/kg)	19.95	44.60
Carbon content (wt%)	37.5	84
Hydrogen content (wt%)	12.5	16
Oxygen content (wt%)	50	0

The sub-models used for developing the 3D CFD model are listed in Table 2.

Table 2. Sub-models used in this study

Name	Sub-model
Turbulence model	RNG k-ε model [18]
Liquid injection	Blob injection model [19]
Spray breakup model	KH-RT model [20]
Drop/wall interaction	Rebound/slide model
Droplets collision model	NTC model [21]
Evaporation model	Frossling model [22]
Wall heat transfer model	O'Rourke and Amsden model [23]
Combustion model	SAGE model [24]
Reaction kinetics	Diesel/methanol dual-fuel mechanism [25]
Soot mechanism	Hiroyasu-NSC model [26]
NO_x mechanism	Extended Zeldovich NO_x model [27]

Although in-cylinder combustion is complex, the three conservation equations of mass (1), momentum (2), and energy (3) constitute the basis for combustion process simulation.

$$\frac{\partial \rho}{\partial t} + \frac{\partial \rho u_i}{\partial x_i} = S \tag{1}$$

$$\frac{\partial \rho u_i}{\partial t}+\frac{\partial \rho u_i u_j}{\partial x_j}=-\frac{\partial P}{\partial x_i}+\frac{\partial \sigma_{ij}}{\partial x_j}+S_i \quad (2)$$

$$\frac{\partial \rho e}{\partial t}+\frac{\partial u_j \rho e}{\partial x_j}=-P\frac{\partial u_j}{\partial x_j}+\sigma_{ij}\frac{\partial u_i}{\partial x_j}+\frac{\partial}{\partial x_j}(K\frac{\partial T}{\partial x_j}) +\frac{\partial}{\partial x_j}(\rho D\sum_m h_m\frac{\partial \Upsilon_m}{\partial x_j})+S \quad (3)$$

The RNG k-ε model was selected to characterize the turbulence, which significantly contributes to the combustion process. The turbulent kinetic energy k and turbulent dissipation rate ε were calculated according to Equations (4) and (5), respectively.

$$\frac{\partial \rho k}{\partial t}+\frac{\partial \rho u_i k}{\partial x_i}=\tau_{ij}\frac{\partial u_i}{\partial x_j}+\frac{\partial}{\partial x_j}\left(\frac{\mu+\mu_t}{\mathrm{Pr}_k}\frac{\partial k}{\partial x_j}\right) -\rho\varepsilon+\frac{C_s}{1.5}S_s \quad (4)$$

$$\frac{\partial \rho \varepsilon}{\partial t}+\frac{\partial(\rho u_i \varepsilon)}{\partial x_i}=\frac{\partial}{\partial x_j}\left(\frac{\mu+\mu_t}{\mathrm{Pr}_\varepsilon}\frac{\partial \varepsilon}{\partial x_j}\right)+C_{\varepsilon 3}\rho\varepsilon\frac{\partial u_i}{\partial x_i} +\left(C_{\varepsilon 1}\frac{\partial u_j}{\partial x_j}\tau_{ij}-C_{\varepsilon 2}\rho\varepsilon+C_s S_s\right)\frac{\varepsilon}{k} +S-\rho R_\varepsilon \quad (5)$$

The SAGE model was chosen to simulate the combustion process based on the skeleton kinetic mechanism for the methanol/n-heptane dual-fuel combustion proposed by Liu et al., which includes 52 species and 182 reactions, and exhibits high accuracy for characterizing dual-fuel combustion [25].

In order to quantify the knocking phenomenon under different operating conditions, the indicator knock index (KI) is chosen, which denotes the average value of PP_{max}(peak-to-peak value of the vibration signal of filtered pressure) for local pressure monitoring points at N different locations [28].

$$KI=\frac{1}{N}\sum_{n=1}^{N}PP_{\max,n} \quad (6)$$

For CFD models that simulate the combustion process with one cycle, it is inappropriate to use the cyclic fluctuation rate of the IMEP to evaluate misfire occurrence. Therefore, referring to the definition of CA10 (combustion initiation angle) and CA90 (combustion termination angle), a new parameter, the Percentage of Combustion Completion (PCC), which is defined as the ratio of the accumulated heat released at the end of the simulation to the theoretical energy input, was introduced to evaluate the misfire phenomenon for CFD modelling. In this study, PCC= 10% and PCC= 90% were set as the boundaries for complete misfire and partial misfire, respectively.

$$PCC=\frac{Q}{m\cdot LHV}\times 100\% \quad (7)$$

3. MODEL SETUP AND VALIDATION

3.1 Model setup

The main engine specifications are presented in Table 3. It is worth mentioning that a number of experiments have been conducted on the investigated dual-fuel engine, while corresponding data acquisition and post-processing can be found in reference [29].

Table 3. Engine specifications.

Parameter	Specification
Engine type	6-cylinder
Displacement (L)	12.149
Bore×stroke (mm)	129×155
Compression ratio	16.5
IVC (°CA ATDC)	-150
EVO (°CA ATDC)	129
Nozzle (number×nozzle diameter) (mm)	8×0.22

In this study, the complete engine model was developed by using the *Make engine sector surface* tool, and the grid was generated automatically using the CONVERGE software. The simulation starts with the -150° CA intake valve closed and ends with the 129° CA exhaust valve open. Because the injector contains eight uniformly distributed nozzles, a one-eighth model of the combustion chamber was constructed to reduce the computational cost by utilizing axial symmetry. According to Figure 2, the simulation results of the two simulation models do not show a significant difference, indicating that both models can satisfy model accuracy validation.

Therefore, after considering the model accuracy and computational cost, the one-eighth model was selected for the subsequent research. Six local pressure monitoring points were set inside the computational domain, as shown in Figure 3.

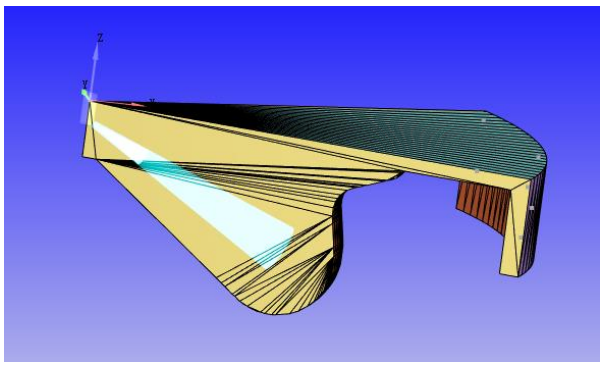

Figure 1: Complete model of the combustion chamber and one-eighth model at TDC.

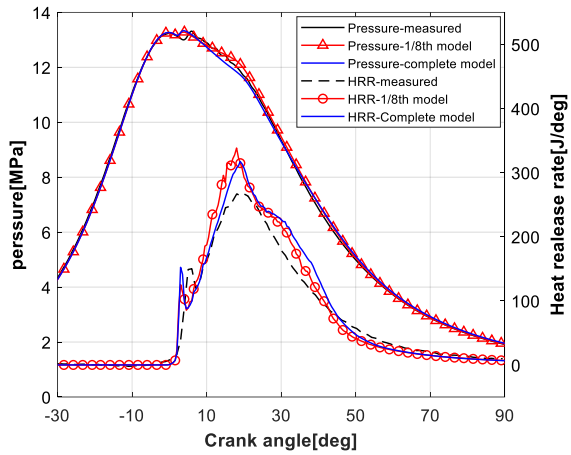

Figure 2: In-cylinder pressure and HRR comparison at 100% operation loads.

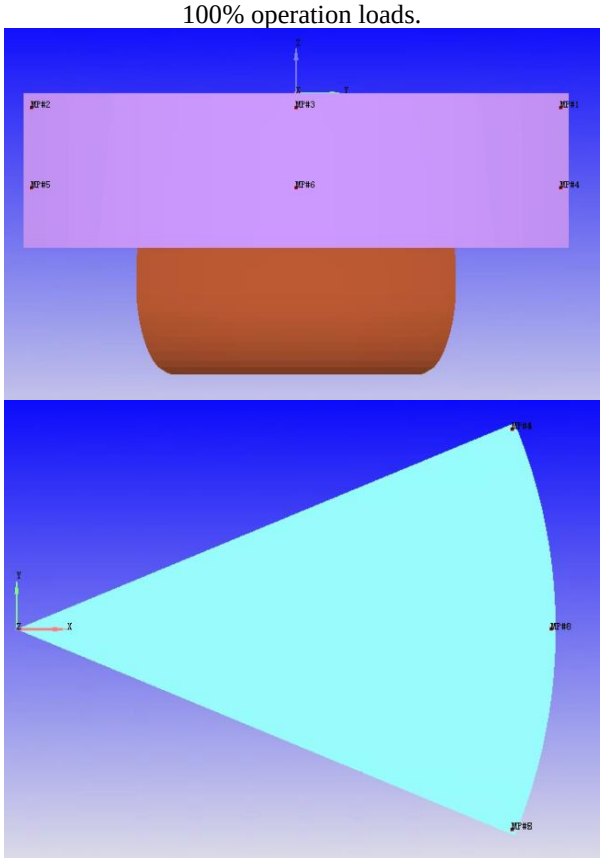

Figure 3: Location of the monitoring points.

3.2 Model validation

Before validating the developed CFD one-eighth model, it is necessary to verify the mesh grid size independence. To determine the appropriate basic grid size, four grid schemes (1.5, 2.0, 2.5, and 3.0 mm) were compared in terms of in-cylinder pressure. Figure 4 shows the comparison results of the pressure for four basic grid sizes. Balancing the prediction accuracy and computation cost, a 2 mm basic grid size and 33689 basic cells were ultimately selected in this study.

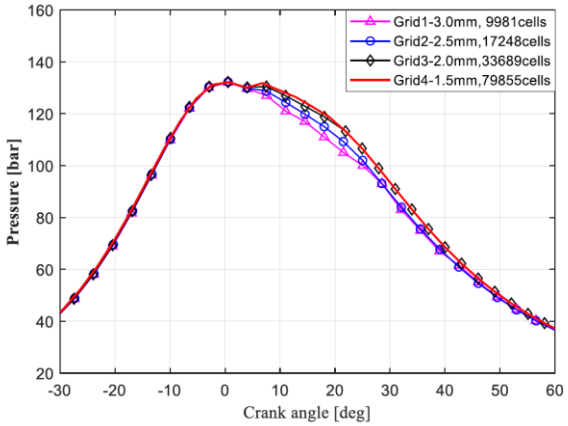

Figure 4: In-cylinder pressure comparison with 4 base grid sizes.

To validate the model accuracy, the simulation results were compared with the experimental data under operation loads of 32%, 53%, 74%, and 100%. However, due to page limitations, the results are not fully presented.

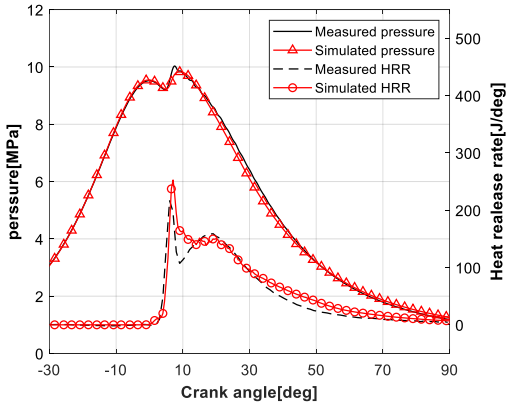

Figure 5: In-cylinder pressure and HRR comparison at 53% operation loads.

The simulated and measured pressures and heat release rate (HRR) at 100% operating conditions are shown in Figures 2, which clearly demonstrate good agreement with each other. It can be observed that under 100% operating conditions the predicted results match the experimentally obtained data with adequate accuracy. Figures 5 and 6 show the accuracy verification of the pressure and HRR at 53% and 32% of the operation loads, respectively.

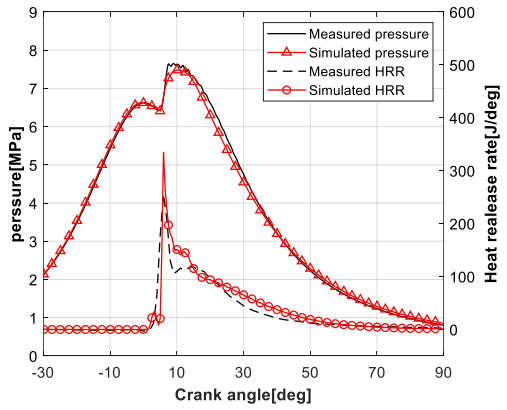

Figure 6: In-cylinder pressure and HRR comparison at 32% operation loads.

This study quantitatively compared the simulated and measured p_{max}, and the corresponding angles (α_1), p_{com}, and IMEP. Comparisons of the simulated and measured in-cylinder parameters at 4 different loads are presented in Table 4. It can be seen that under 100% load, the simulated peak pressure was 132.8 bar, compared with the measured peak pressure of 133.1 bar, the error is only 0.2%, and the corresponding angle difference is 1.89 °CA. The simulated p_{com} was 132.6 bar, which is very close to the experimental data of 132.4 bar, with an error of 0.2%. The relative errors of all the parameters at the other operating loads were less than 5%, and the angles were less than 3°CA, indicating that the model was more accurate in terms of combustion.

Table 4. Quantitative Comparison between the simulated and measured in-cylinder parameters

Load	Parameters	p_{max} (bar)	α_1	p_{com} (bar)	IMEP (bar)
100%	Simulation	132.8	4.03	132.6	19.78
	Experiment	133.1	5.92	132.4	18.90
	Error	0.2%	1.89	0.2%	4.6%
74%	Simulation	128.4	5.64	128.1	17.89
	Experiment	128.0	6.23	127.4	18.00
	Error	0.3%	0.59	0.5%	0.6%
53%	Simulation	99.37	9.02	94.87	11.84
	Experiment	100.1	7.80	95.06	12.39
	Error	0.7%	1.22	0.2%	4.4%
32%	Simulation	74.81	10.5	66.15	9.37
	Experiment	76.05	9.49	65.59	9.70
	Error	1.6%	1.01	0.9%	3.4%

A comparison of the simulated and measured emissions under 4 different operating conditions is presented in Table 5. It can be observed that the relative errors for both NOx and CO are less than 10%, whereas HC has larger relative errors, except at the100% load. Combined with the higher simulated NOx emissions, the overestimated temperature may have been the main cause. Overall, the accuracy of emission predictions of the model was acceptable.

Table5. Comparison between the simulated and the measured emissions.

Load	Parameters	NOx (g/kWh)	CO (g/kWh)	HC (g/kWh)
100%	Experiment	1.83	6.82	17.67
	Simulation	1.67	7.47	18.8
	Error(%)	8.74	9.53	6.4
74%	Experiment	1.34	9.36	32.45
	Simulation	1.47	8.55	28.40
	Error(%)	9.70	8.65	12.48
53%	Experiment	1.50	7.21	24.93
	Simulation	1.62	6.50	22.30
	Error(%)	8.80	9.85	10.55
32%	Experiment	1.62	3.77	10.30
	Simulation	1.70	3.45	8.90
	Error(%)	4.94	8.49	13.59

In summary, by comparing the p_{max}, HRR, IMEP, and emissions obtained from the simulation and experiments, it was proven that the developed model has sufficient accuracy and can be used in subsequent research.

4. RESULTS AND ANALYSIS

In this section, the validated 3D model is used to investigate the maximum methanol substitution rate under different operating conditions, the effects of the MSR on engine performance, and a comparison between diesel/methanol and diesel/natural gas dual-fuel modes.

4.1 Maximum methanol substitution rate under different operating loads

In this study, the maximum methanol substitution rate (MMSR) under four operating conditions (25%, 50%, 75%, and 100% load) was identified by considering the misfire and knocking occurrences. Figure 7 shows that the MMSR tended to increase from 5% to 43% when the operating load increased from 25% to 75% and then decreased to 20% at 100% operating load. Misfire and knocking were the main factors constraining the MMSR at low and high operating loads, respectively, as shown in Figures 8 and 9.

Figure 8 presents the PCC variation with methanol substitution rate (MSR) at different operating loads. As described in Equation (7), the partial misfire and complete misfire limits are defined as PCC = 90% and PCC=10%, respectively. In this study, the partial misfire limit was used to determine the maximum methanol substitution rate at low operating loads. At 25% and 50% operating loads, the PCC showed a decreasing trend with increasing MSR, which constrained the MMSR to 5% and 25%, respectively. For the case of 25% operating load, the PCC drops below 10% at

approximately 50% MSR, indicating complete misfire occurrence. At 75% and 100% operating loads, the PCC exhibited an increasing trend with increasing MSR, which was probably caused by the increasing intake pressure and temperature. This means that the methanol addition stimulates combustion; thus the partial misfire limit is no longer the MMSR constraint at high operating loads.

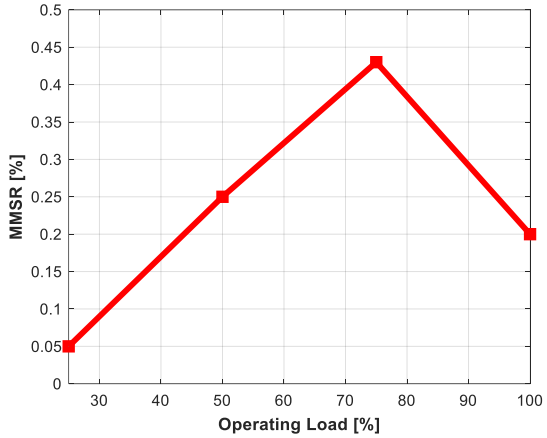

Figure 7: MMSR variation with engine operating load.

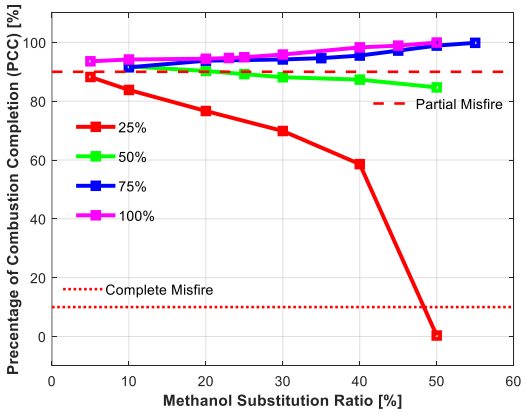

Figure 8: PCC variation with MSR under different operating loads.

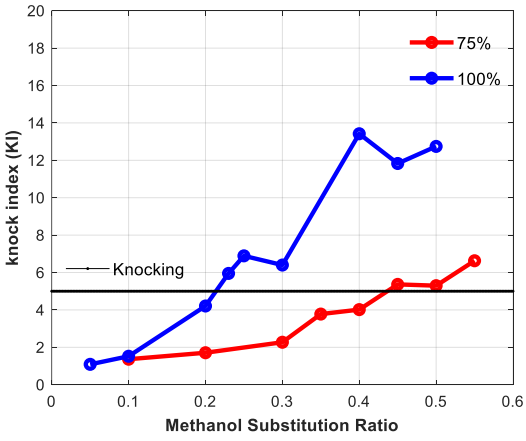

Figure 9: Knocking condition of engine.

However, with an increase in the operating load, the combustion becomes more violent with increasing MSR, which makes the knocking index (KI) the main factor constraining the MMSR at high operating loads. Figure 9 shows the KI variation with MSR under 75% and 100% operating loads. At high operating loads, the MMSR can be obtained by identifying the knocking index. Currently, the setting of KI is mainly based on SI engines and is not applicable to this study. In this study, first, the monitoring points were all close to the cylinder wall, resulting in a larger KI; second, in the pure diesel mode KI=2.52, so KI of the knocking limit should be larger. Finally, it was concluded from the analysis of the results that a significant difference in the cylinder pressure curves (shown in Figure 10) was observed at the 75% work and 50% MSR condition, which was considered to be closer to the knockout boundary (KI=5). In summary, KI=5 was tentatively selected as the limiting value for this study. As shown in Figure 9, the MMSR at the 75% and 100% operating loads were approximately 43% and 20%, respectively.

4.2 Effects of methanol substitution rate on engine performance and emissions

Among the investigated 4 operating loads, the largest MMSR was achieved under 75% operating load, which was the most economical operating point for engine management. Thus, the effects of different MSR on engine combustion and emissions were analyzed under a 75% operating load.

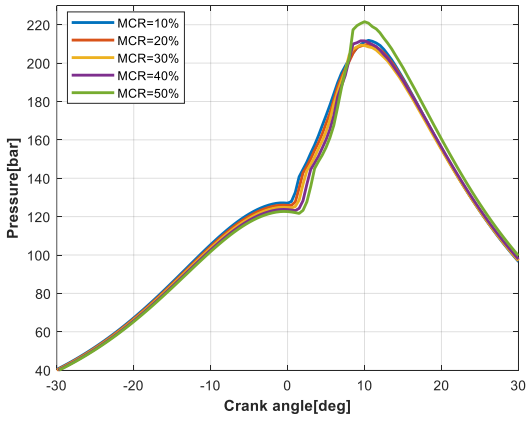

Figure 10: Comparison of in-cylinder pressure.

As shown in Figures 10 and 11, both the in-cylinder temperature and pressure during the compression stage decrease with increasing MSR, which is caused by the increase in the specific heat capacity of the in-cylinder gas owing to the increase in methanol. After diesel injection, it can be observed that as the MSR increases, the ignition delay period increases with a shorter combustion duration, indicating that the in-cylinder combustion becomes more intense, which can also be observed from KI. The two factors together resulted in a

decrease and then an increase in the maximum pressure and temperature.

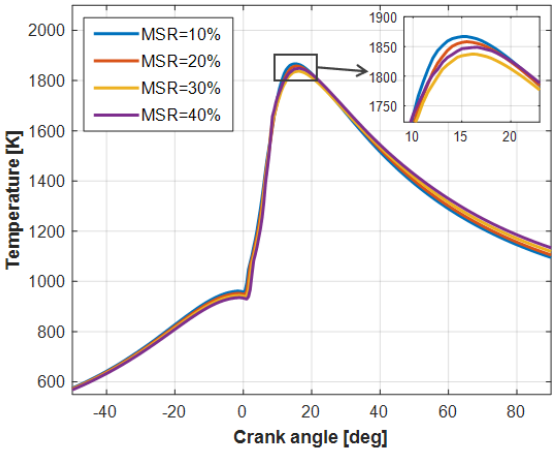

Figure 11: Comparison of in-cylinder temperature.

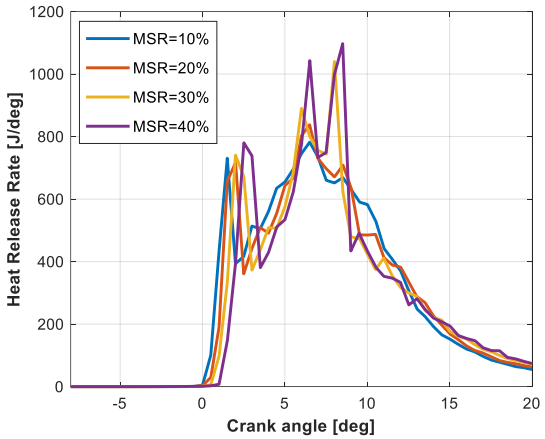

Figure 12: Comparison of heat release rate.

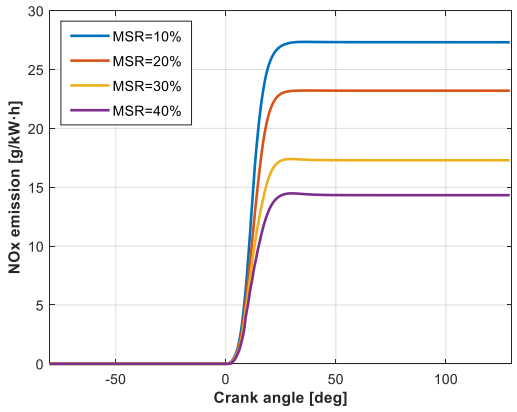

Figure 13: Comparison of NO_x emission.

A comparison of the HRR is shown in Figure 12, which shows that the HRR gradually changes from double to triple peaks as the MSR increases. It was observed that when the MSR was small, the combustion process mainly consisted of two stages: premixed combustion and diffusion combustion of diesel fuel. With a gradual increase in the MSR, the premixed combustion of methanol played a more important role in the combustion process, which contributed to the change from double to triple peaks. The HRR and KI analyses suggest that the engine is already at slight knocking at approximately 40% MSR, which might be beneficial to the output power [30]. Figure 13 shows the NO_x emission variation with MSR. It can be seen that NOx emissions decreased significantly with increasing MSR. There are two possible reasons for this: first, the reduction in diesel injection leads to a reduction in the hot zone at the flame front, and second, methanol combustion has an inhibitory effect on NOx production.

4.3 Comparison of diesel/methanol and diesel/natural gas dual fuel mode

In this section, a comparison is made between the diesel/methanol and diesel/natural gas dual-fuel modes in terms of combustion and emissions performance. Because the largest MMSR was achieved at 75% operating load, the operation mode comparison was conducted at 75% operating load. In addition, a maximum methanol substitution rate of 43% was used for the diesel/methanol mode, whereas a maximum natural gas substitution rate of 90% was used for the diesel/natural gas prototype mode.

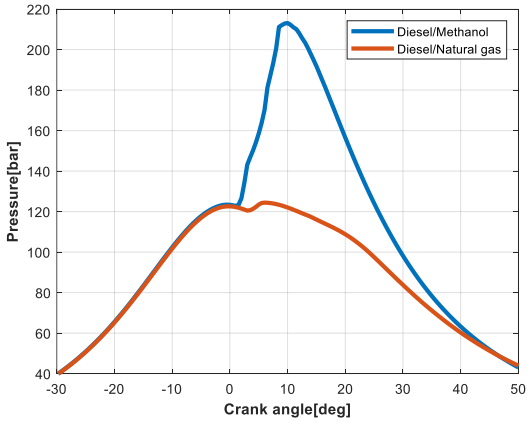

Figure 14: Comparison of in-cylinder pressure.

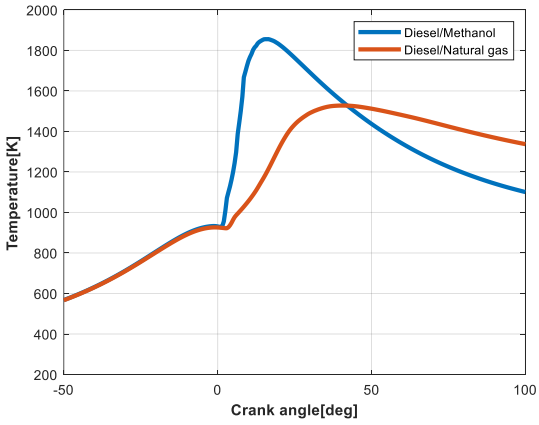

Figure 15: Comparison of in-cylinder temperature.

As shown in the Figures 14 and 15, the maximum pressure and temperature of the

diesel/methanol mode are much higher than those of prototype mode, which could probably increase the engine's mechanical and thermal loads. Figure 16 shows a comparison of the HRR. With the same pilot injection timing, the diesel/methanol mode exhibited shorter ignition delay and combustion duration. Besides, the combustion phase advanced with three HRR peaks in diesel/methanol mode. Compared with the diesel/natural gas mode, the higher temperature resulted in a significant increase in NO_x emissions in the diesel/methanol mode, as shown in Figure 17.

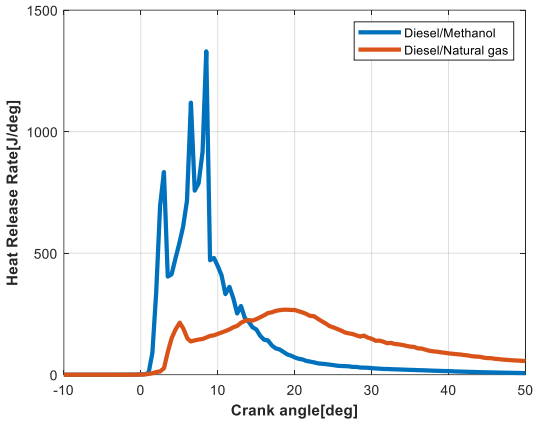

Figure 16: Comparison of heat release rate.

Figure 18 shows a comparison of the in-cylinder temperature distributions of the diesel/methanol and diesel/natural gas modes. As diesel is used mainly as a pilot fuel (approximately 10% energy percentage) in the diesel/natural gas mode, the diesel penetration distance is much smaller than that in the diesel/methanol mode, which uses 57% diesel for combustion. Owing to the shorter diesel spray penetration, the diesel/natural gas mode exhibited a significant afterburning phenomenon. However, diesel accounts for 57% of the total heat release; thus, the injection mass and spray penetration are much larger than those in the diesel/natural gas mode. Therefore, the combustion phase was advanced, thereby improving the afterburning phenomenon. It can also be observed that the main factor responsible for the high NO_x emissions in the methanol mode is excessive diesel injection.

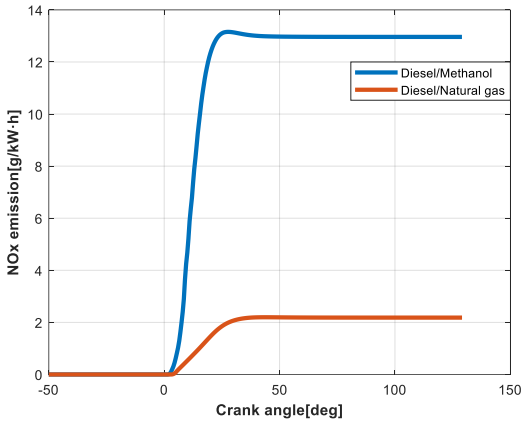

Figure 17: Comparison of NO_x.

Combining the simulation results of Figures 16 and 18, it can be found that for the diesel/methanol dual-fuel engine, the combustion was completed at approximately 20° CA; but from the three-dimensional results, there still exists a considerable amount of space in the low-temperature state (approximately 1500 K). For a diesel/natural gas dual-fuel engine, the temperature of the burned zone of the natural gas is very high (approximately 2000 K). In summary, it was concluded that methanol combustion contributes very little to the temperature increase, and therefore, NO_x generation can be effectively suppressed.

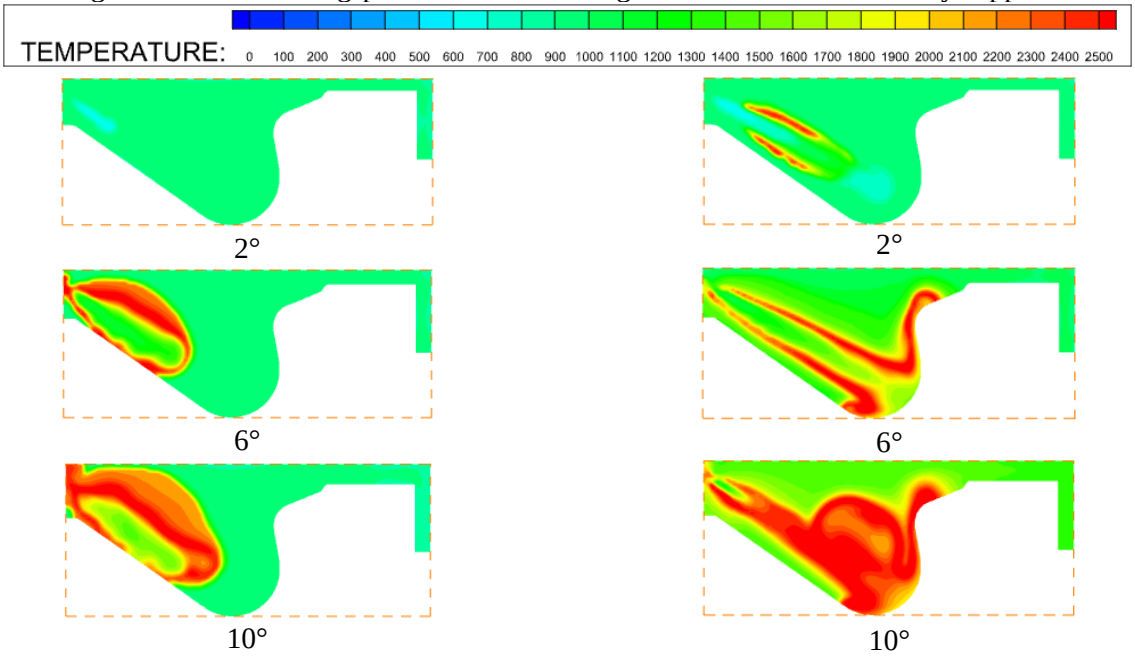

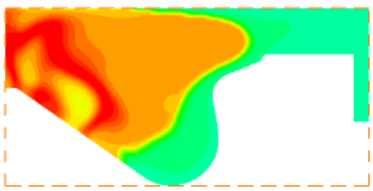

a.Natural gas-diesel dual fuel engine.

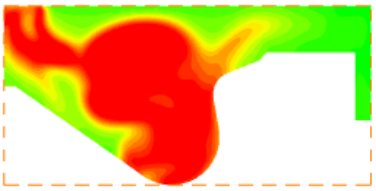

b.Methanol-diesel dual fuel engine.

Figure 18: In-cylinder temperature distribution of different fuel engines.

5. CONCLUSION

In this study, a 3D CFD simulation model of a diesel/methanol dual-fuel engine was developed to investigate the maximum methanol substitution ratio under different operating conditions, the effects of the MSR on engine performance, and a comparative study with the diesel/natural gas dual-fuel operation mode. The conclusions are as follows.

1. For the diesel/methanol dual-fuel engine in the inlet port injection mode, the MMSR tended to increase and then decrease with an increasing operating load. The MMSRs at 25%, 50%, 75% and 100% loads are 5%, 25%, 43% and 20%, respectively.

2. At 75% operation condition, with the increase in MSR, the ignition delay period increased and the combustion duration decreased, resulting in more complete combustion and better emissions.

3. Compared with the prototype, the ignition delay and combustion duration of the diesel/methanol dual-fuel mode were significantly shorter, resulting in better engine dynamics for the same total heat release. Higher pressures and average temperatures mean increased mechanical and thermal loads, which may limit the engine's operating range. In addition, diesel/methanol dual-fuel engines have worse NO_x emissions.

4. In the diesel/methanol mode, methanol combustion is very rapid and the contribution to the temperature increase after combustion is not obvious; at the end of combustion, there is still a considerable space in the cylinder at approximately 1500 K. Therefore, the application of methanol in the engine can effectively inhibit the generation of NO_x.

5. As fuel, methanol can reduce NO_x generation in two ways: first, the use of methanol to replace diesel fuel can reduce the in-cylinder hot zone caused by diesel fuel combustion; second, the combustion of methanol does not have a significant effect on the temperature increase, and the relatively low temperature of the combusted zone can inhibit NO_x generation.

Owing to the limitations of knocking and misfire, there is an upper limit to the substitution rate of methanol, which is much lower than that of natural gas without changing the original engine structure. Nevertheless, as a new alternative fuel, methanol still exhibits unique advantages such as a faster combustion speed and stronger NOx suppression ability. In response to these findings, future research will focus on a diesel/methanol dual-fuel mode with direct in-cylinder injection to improve engine combustion and emission performance while increasing the methanol substitution rates.

6. ACKNOWLEDGMENTS

This study was supported by the National Key Research and Development Program of China (No. 2022YFE0107200).

REFERENCE

[1] Tian Z et al, “The effect of methanol production and application in internal combustion engines on emissions in the context of carbon neutrality: A review,”. *Fuel*, vol.320, no.123902, Jul.2022.

[2] Gong C et al, “Numerical study of twin-spark plug arrangement effects on flame, combustion and emissions of a medium compression ratio direct-injection methanol engine,”. *Fuel*, vol.279, no.118427, Nov.2020.

[3] Duan Q et al, “Experimental study of knock combustion and direct injection on knock suppression in a high compression ratio methanol engine,”. *Fuel*, vol.311, no.122505, Mar.2022.

[4] Yang S et al, “Combustion and emissions characteristics of methanol/gasoline CISI engines under different injection modes,”. *Fuel*, vol.333, no.126506, Feb.2023.

[5] Tian Z et al, “Numerical comparative analysis on performance and emission characteristics of methanol/hydrogen, ethanol/hydrogen and butanol/hydrogen blends fuels under lean burn conditions in SI engine,”. *Fuel*, vol.313, no.123012, Apr.2022.

[6] Zhang Z et al, “Investigation on the combustion and emission characteristics of diesel engine fueled with diesel/methanol/n-butanol blends,”. *Fuel*, vol.314, no.123088, Apr.2022.

[7] Fan C et al, “Chemical feature of the soot emissions from a diesel engine fueled with methanol-diesel blends,”. *Fuel*, vol.297, no.120739, Aug.2021.

[8] EL-Seesy A I et al, “Enhancement of the combustion and stability aspects of diesel-

methanol-hydrous methanol blends utilizing n-octanol, diethyl ether, and nanoparticle additives,". *Journal of Cleaner Production*, vol.371, no.133673, Oct.2022.
[9] Xu C et al, "Effect on the performance and emissions of methanol/diesel dual-fuel engine with different methanol injection positions,". *Fuel*, vol.307, no.121868, Jan.2022.
[10] Tao W et al, "The effect of diesel pilot injection strategy on combustion and emission characteristic of diesel/methanol dual fuel engine,". *Fuel*, vol.324, no.124653, Sep.2022.
[11] Liu J et al, "Experimental study on effects of pilot injection strategy on combustion and emission characteristics of diesel/methanol dual-fuel engine under low load,". *Energy*, vol.247, no.123464, May.2022.
[12] Panda K et al, "Diesel injection strategies for reducing emissions and enhancing the performance of a methanol based dual fuel stationary engine,". *Fuel*, vol.289, no.119809, Apr.2021.
[13] Yin X et al, "A comparative study on operating range and combustion characteristics of methanol/diesel dual direct injection engine with different methanol injection timings,". *Fuel*, vol.334, no.126646, Feb.2023.
[14] Li Z et al, "An exploratory numerical study of a diesel/methanol dual-fuel injector: Effects of nozzle number, nozzle diameter and spray spacial angle on a diesel/methanol dual-fuel direct injection engine,". *Fuel*, vol.318, no.123700, Jun.2022.
[15] Wang Y et al, "Study on the performance of diesel-methanol diffusion combustion with dual-direct injection system on a high-speed light-duty engine,". *Fuel*, vol.317, no.123414, Jun.2022.
[16] Li Z et al, "To achieve high methanol substitution ratio and clean combustion on a diesel/methanol dual fuel engine: A comparison of diesel methanol compound combustion (DMCC) and direct dual fuel stratification (DDFS) strategies,". *Fuel*, vol.304, no.121466, Nov.2021.
[17] Sun W et al, "Numerical study of injection strategies for marine methanol/diesel direct dual fuel stratification engine,". *Journal of Cleaner Production*, vol.421, no.138505, Oct.2023.
[18] Han Z et al, "Turbulence modeling of internal combustion engines using RNG κ-ε models,". *Combustion Science and Technology*, vol.106, no.4, pp.267-295, Mar.1995.
[19] Reitz R D et al, "Structure of high-pressure fuel sprays,". *SAE Transactions*, vol.96, no.5, pp.492-509, 1987.
[20] Beale J C et al, "Modeling spray atomization with the Kelvin-Helmholtz/Rayleigh-Taylor hybrid model,". *Atomization and Sprays*, vol.9, no.6 pp.623-650, 1999.
[21] Naber J D et al, "Modeling engine spray/wall impingement,". *SAE Transactions*, vol.97, no.6, pp.118-140, 1988.
[22] Amsden, O'Rourke, and Butler, "KIVA-II: A Computer Program for Chemically Reactive Flows with Sprays," Los Alamos National Laboratory Technical Report LA-11560-MS, 1989.
[23] Amsden, "KIVA-3V: A Block Structured KIVA Program for Engines with Vertical or Canted Valves," Los Alamos National Laboratory Technical Report LA-13313-MS, 1997.
[24] Senecal P K et al, "Multi-dimensional modeling of direct-injection diesel spray liquid length and flame lift-off length using CFD and parallel detailed chemistry,". *SAE Transactions*, vol.112, no.3, pp.1331-1351, 2003.
[25] Liu S, Sun T et al, "A new skeletal kinetic model for methanol/n-heptane dual fuels under engine-like conditions,". *Energy*, vol.263, no.125648, Jan.2023.
[26] Hiroyasu H et al, "Models for combustion and formation of nitric oxide and soot in direct injection diesel engines,". *SAE Transactions*, vol.85, no.1, pp.513-526, 1976.
[27] Heywood J B, "Internal combustion engine fundamentals," 2018.
[28] Liang L et al, "Modeling knock in spark-ignition engines using a G-equation combustion model incorporating detailed chemical kinetics," Tech. rep. 2007-01-0165. Ford Research and Advanced Engineering, University of Wisconsin-Madison, Wisconsin, United States, 2007.
[29] Xiang L et al, "Parametric investigation on the performance-emissions trade-off and knocking occurrence of dual fuel engines using CFD,". *Fuel*, vol.340, no.127535, May.2023.
[30] Bi F et al, "Knock detection based on the optimized variational mode decomposition," *Measurement*, vol.140, pp.1-13, Jul.2019.
[31] Li Y et al, "Thermodynamic energy and exergy analysis of three different engine combustion regimes,". *Applied Energy*, vol.180, pp.849-858, 2016.